



Implicit-explicit higher-order time integration schemes for computations of structural dynamics with fluid-structure interaction

José C. Pedro¹, Mapundi K. Banda² and Precious Sibanda³

¹Departamento de Matemáticas
da Faculdade de Ciências
Universidade Agostinho Neto
Caixa Postal n° 815, Avenida 4 de Fevereiro n°71
Luanda, Angola
caluynal@hotmail.com

²Department of Mathematics and Applied Mathematics
University of Pretoria
Private Bag X20, Hatfield 0028, South Africa
mapundi.banda@up.ac.za

³School of Mathematics, Statistics and Computer Science
University of Kwazulu Natal
Private Bag X01, Scottsville 3209, South Africa
sibandap@ukzn.ac.za

Received: September 3, 2014; Accepted: February 15, 2015

Abstract

In this paper higher order implicit Runge-Kutta schemes are applied to fluid-structure interaction (FSI) simulations. A staggered approach with a structural predictor is applied to an FSI problem. The equations governing the dynamics of the structure are integrated in time by the Explicit Single Diagonal Implicit Runge-Kutta (ESDIRK) schemes and the arbitrary high order finite volume scheme is taken as the fluid solver. The performance of the ESDIRK scheme of order of convergence three to five is tested. Comparative studies with other time integration schemes which have been successfully applied to FSI problems are undertaken. Comparisons to test the performance of the scheme are carried out. The staggered approach is applied to couple the structure and the compressible fluid, therefore the added mass effect is not considered. However the influence of the structural predictors is analyzed through energy conservation.

Keywords: Fluid-structure interaction; ESDIRK; High order time integration; Structural predictor; Structural dynamics; staggered approach; Euler gas dynamics; piston problem

MSC2010 No: 74F10, 35Q31, 65L06

1. Introduction

The staggered approach is one of the schemes often used to solve fluid-structure interaction (FSI) problems. In this approach the fluid and the structure are integrated alternating in time by separate solvers, Blom (1998). The coupling between the fluid and structure is realized through boundary conditions. Several versions of the staggered scheme exist depending on the problem being solved, see Mouro (1996); Park et al. (1997); Pedro et al. (2012); Piperno (1997) and Prananta and Houjet (1996). For example, in Prananta Houjet (1996) a staggered scheme was used for transonic flutter calculations; in [Mouro (1996)] it was used for incompressible fluid-structure interaction; in Piperno (1997) staggered approaches using a structural predictor were developed.

The structure predictors allow a significant reduction in the energy dissipation, Piperno (1997). In this paper, a staggered approach with structure predictor will be extended to higher-order schemes and, as a test case, will be applied to the familiar piston problem.

In this paper, the system modelling the FSI problem is composed of two subsystems: the fluid subsystem that is governed by nonlinear Euler equations and the structure subsystem governed by a one-degree of freedom system is considered. In general, in the existing literature, the staggered approach is set up as follows: the solution of the structure is based on schemes with at most second-order time accuracy while the fluid flow solvers are at most second-order based on the finite volume or the finite element methods (FVM or FEM) as the case may be. In integrating the structure, the Newmark schemes are the most preferred. In Piperno et al. (1995) the dynamic response of a flexible structure in fluid flow was solved using a second-order accurate midpoint rule for the structure. In [Piperno (1997)] the supersonic flutter of a flat panel was simulated, using the trapezoidal rule (Newmark with parameters $\beta = 1/4$, $\gamma = 1/2$) for the structure. In Blom (1998) the time marching computational fluid-structure interactions algorithms in which the structure was integrated numerically by an average acceleration scheme was investigated. This scheme is the optimal case of the Newmark method [Bathe and Wilson (1976)] with no numerical damping and unconditional stability. In Farhat and Lesoinne (2000) coupled transient aeroelastic problems with the flutter analysis of the AGARD Wing 445 were solved: the structure system is advanced by the second-order time accurate midpoint rule.

In Michler_et_al. (2003) the relevance of maintaining conservation for a model fluid-structure interaction problem was investigated, using the Newmark method with the parameter choice of $\beta = 1/4$, $\gamma = 1/2$ for structure. The same scheme was employed in Michler et al. (2004) to compare the partitioned (staggered) and monolithic (in which the structure and fluid flow problems are solved simultaneously) solution procedures for the numerical simulations of fluid-structure interactions.

Most recently in Lefrançois and Boufflect (2010) a review was presented which provided a basic and solid discussion of numerical issues underlying the physics of fluid-structure interaction, employing the Newmark-Wilson scheme as the structure solver. In Garelli (2011) coupling strategies for fluid-structure interaction were investigated and the average acceleration scheme to integrate the structure in time was used.

In Zuijlen and Bijl (2005) a higher-order time integration scheme was introduced where the Explicit Single Diagonally Implicit Runge-Kutta (ESDIRK) was applied to FSI problems for the first time in the framework of the staggered approach. The ESDIRK was shown to have clear advantages in terms of reducing drift in resolving the structure solution as well as efficiency and higher-order accuracy. The scheme was applied to isentropic fluid flow as well as systems resulting from small perturbations of the governing *i.e. equations were linearized*. In this paper, extensions to this approach are adopted: for time integration of the structure ESDIRK schemes of the order three to five are proposed; for the flow an arbitrary high order finite volume scheme is employed.

In coupling the fluid and the structure solutions, two different structure predictors are considered. The idea is to demonstrate their performance in decreasing additional fictitious energy. Tests are performed on different natural frequencies of the structure. This extended algorithm is applied to the piston problem which has a one-degree of freedom and the nonlinear Euler equation of gas dynamics is employed for the gas in the piston. The results show that these higher-order accuracy solvers have the capability to eliminate spurious effects due to the numeric and give high-order accurate solutions efficiently. The problem considered in developing these schemes is one-dimensional and other challenges in higher spatial dimensions, such as grid entanglement may result. In addition adaptive as well as unstructured grids might be desirable. In this preliminary study care has been taken to select a finite volume scheme for the fluid solver which has the potential to be adapted to more spatial dimensions with high-order accurate solution [Dumbser et al. (2007), Dumbser and Käser (2007)]. Investigations for averting grid entanglement are a subject for future research.

In summary, the physical test problem is presented in Section 2. This includes the mathematical model of the problem. In Section 3 numerical methods and requisite extensions are presented. The paper ends with the numerical results in Section 4 as well as a discussion of the results and suggestions for future work in Section 5.

2. Statement of the Problem

In this section, we introduce the case study that will be used to test the numerical methods that have been developed for the FSI problem. The physical problem will be introduced followed by the mathematical models used to describe the problem.

2.1. The physical problem

We consider a compressible fluid contained in a tube, with its left-hand side closed by a fixed wall and its right-hand side closed by a moving piston, as depicted in Figure 2.1.

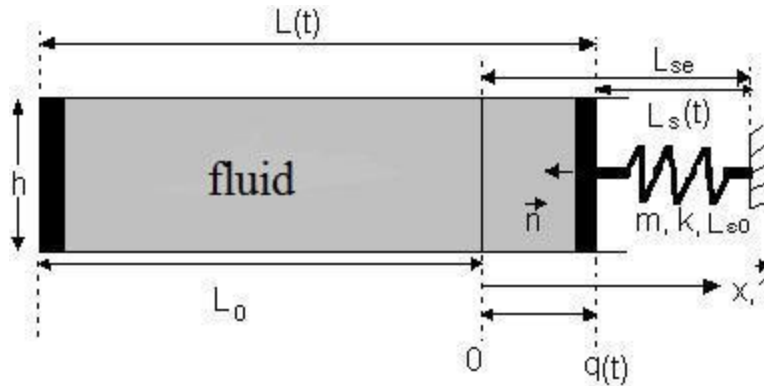


Figure 2.1. A compressible fluid in a tube with a moving piston

The piston with mass m is supported by a spring which has stiffness k . There are three different lengths that define the spring, namely, un-stretched denoted by (L_{s0}) , at rest under pressure denoted by (L_{se}) , and at a given time t during the fluid-structure interaction process denoted by $(L_s(t))$. Further, at time t , the displacement, velocity and acceleration of the piston confined to its position at rest are denoted by $q(t)$, $\dot{q}(t)$, and $\ddot{q}(t)$ respectively. The fluid in the tube is modeled as one-dimensional inviscid and compressible, with variations only in the x direction, and is defined by its density ρ , velocity u , and pressure p . The gas contained in the tube is air which is initially at rest at pressure p_0 . The length of the chamber at rest is defined by L_0 and at time t is $L(t) = L_0 + q(t)$.

In the following sub-sections, the mathematical models depicting the physical problem presented above will be presented. Firstly, the structure subsystem followed by the fluid subsystem as well as the coupling of the fluid and structure subsystems will be presented.

2.2. The Structure subsystem

The movement of the piston is governed by the following equation

$$m\ddot{q} + kq = f_{ext}(t); \quad (2.1)$$

With

$$q(0) = q_0 \text{ and } \dot{q}(0) = 0,$$

where q and \ddot{q} are the displacement and acceleration of the piston, respectively. The external force $f_{ext}(t)$ is equal to the pressure difference between the ambient pressure p_0 and the pressure in the fluid domain at the interface $p(t)$, multiplied by the piston surface, A :

$$f_{ext}(t) = A(p(t) - p_0). \quad (2.2)$$

For such a one-dimensional problem the area, A , is normalized to unity.

2.3. The Fluid subsystem

The fluid is governed by the one-dimensional nonlinear Euler equations of gas dynamics, corresponding to the conservation laws:

$$\frac{\partial}{\partial t} \begin{pmatrix} \rho \\ \rho u \\ \rho E \end{pmatrix} + \frac{\partial}{\partial x} \begin{pmatrix} \rho u \\ \rho u^2 + p \\ u(\rho E + p) \end{pmatrix} = 0, \quad (2.3)$$

where ρ , u , E and p are the density, the velocity, the total energy and pressure, respectively. The equations are closed by the equation of state (EOS) for a perfect gas

$$p = (\gamma - 1)\rho[E - \frac{1}{2}u^2]. \quad (2.4)$$

Since the piston is moving in time, one needs to apply a moving mesh/grid in order to study the fluid flow in the gas chamber. Therefore, the Euler equations must be described on a general moving coordinate system. Thus the equations are described using the arbitrary Lagrangian Euler (ALE) approach [Donea et al. (1982)]. The Euler Equations (2.3) on a moving mesh take the form:

$$\frac{\partial}{\partial t} \int_{\Omega(t)} U d\Omega + \int_{\Omega(t)} \frac{\partial F}{\partial x} d\Omega(t) = 0, \quad (2.5)$$

where the state vector U and the flux F are given by

$$U = \begin{pmatrix} \rho \\ \rho u \\ \rho E \end{pmatrix}; \quad F = \begin{pmatrix} \rho(u - w_x) \\ \rho u(u - w_x) + p \\ \rho E(u - w_x) + up \end{pmatrix}, \quad (2.6)$$

where $u - w_x$ is the contravariant velocity and w_x denotes the coordinate velocity. Equation (2.5) is enclosed by the equation of state for a perfect gas (2.4).

2.4. Coupling fluid and structure

The fluid and the structure are coupled through the external force, Equation (2.2), and the given boundary conditions on the fluid. The boundary conditions for the fluid are described as follows:

$$u(0, t) = 0 \quad \text{and} \quad u(L(t), t) = \dot{q}, \quad (2.7)$$

where \dot{q} is the velocity of the piston.

The first boundary condition describes the velocity at the fixed wall on the left-hand side of the piston at $x = 0$ and the second defines the interface with the piston at $x = L(t)$.

In the following section the numerical approach used to solve the FSI problem described above will be discussed.

3. A Numerical Scheme for FSI

The numerical scheme used to resolve the FSI problem described in Section 2 will be described below. The numerical scheme consists of three parts since a staggered approach is employed. The time integration of the structure problem will be introduced first. The ESDIRK approach is used due to its accuracy and capability to eliminate numerical artefacts such as drift as demonstrated in the results section below, Section 4. Subsequently spatial discretization based on Weighted Essentially Non-Oscillatory (WENO) for fluid flow is discussed. Then time integration of the flow is introduced. The section closes with discussions on two approaches to couple the fluid and structure solvers. A comparative study of these two approaches will be discussed in Section 4.

3.1. Structure Dynamics High Order Integration Schemes

Given a system of the form

$$\dot{q} = F(q, t), \quad (3.1)$$

describing structural dynamics as presented in Equation (2.1). The structural high order time integration we consider in this paper is the explicit single diagonal implicit Runge-Kutta (ESDIRK) approach, which is an L-stable, implicit scheme with an explicit first stage, Zuijlen and Bijl (2005). These characteristics make the implicit stages second order accurate. For every k stage, the following is evaluated:

$$q^{(n)} = q^n + \Delta t \sum_{i=1}^k a_{ki} F^{(i)}, \quad k = 1, \dots, s, \quad (3.2)$$

where $F^{(i)} = F(q^{(i)})$ is the flux at stage i . After computing the s stages, we compute the solution at the next time level by

$$q^{n+1} = q^n + \Delta t \sum_{i=1}^s b_i F^{(i)}. \quad (3.3)$$

The third to fifth order ESDIRK scheme is considered, which consists of four, six and eight stages, respectively. The coefficients a_{ki} and b_i are presented in a Butcher tableau, Kennedy and Carpenter (1987). (See Table 3.1).

Table 3.1. Butcher tableau representing four stages ($s = 4$)

c_1	0	0	0	0
c_2	a_{21}	a_{22}	0	0
c_3	a_{31}	a_{32}	a_{33}	0
c_4	a_{41}	a_{42}	a_{43}	a_{44}
	b_1	b_2	b_3	b_4

At stage $k = i$ the time level $t^{(i)}$ follows from $t^{(i)} = t^n + c_i \Delta t$, where the coefficient $c_i = \sum_j a_{ij}$. As shown by the Butcher tableau, when applying ESDIRK schemes, since the first stage is explicit, there are $s - 1$ implicit stages, which implies solving $s - 1$ implicit systems in one time step.

3.2. Fluid flow space discretization

The fluid flow equations are formulated in the Arbitrary-Lagrangian Eulerian (ALE) framework, to cope with moving meshes, [Farhat et al. (2001)]. The pressure is given according to the ideal gas law (see Equation (2.4)). A finite volume WENO discretization is employed. The method is the one-dimensional case of high order finite volume methods described in detail in Dumbser et al. (2007) and Dumbser Käser (2007). Since the original methods were applied to two and three dimensional hyperbolic systems, throughout this paper this method will be referred as QFENOFV meaning quadrature free essentially non-oscillatory finite volume, as in Dumbser (2007). Next, we give an overview of the method. For further details we refer to Dumbser et al. (2007); Dumbser and Käser (2007) and Shu and Jiang (1996).

3.2.1. Point-wise WENO reconstruction

In a finite volume scheme, we need to compute fluxes across the element interfaces. For this purpose, numerical flux functions are used, which need two point values of the numerical solution at the cell interface, $x_{i+\frac{1}{2}}$, one extrapolated to the interface from the left-side and another one from the right-side. The WENO method produces a higher order accurate point-wise reconstruction of the solution at the cell interface, $x_{i+\frac{1}{2}}$. The general idea of the WENO scheme given by Shu and Jiang (1996) is as follows: In order to obtain a k_{th} order accurate WENO scheme, called $WENO_k$, it is necessary to employ a piecewise reconstruction polynomial of degree $M = k - 1$ for each cell $C_i = [x_{i-\frac{1}{2}}, x_{i+\frac{1}{2}}]$. To calculate the unknown coefficients of the reconstruction polynomial from the known cell averages U_j^n , one needs a *reconstruction stencil* or a *stencil*

$$S_i^M = \cup_{j=i-e}^{i+e} I_j, \quad (3.4)$$

composed of $k = 2e + 1$ elements, where e is the extension of the stencil to the left and the right, M is the degree of the reconstruction polynomial and i is the i_{th} grid cell. The reconstruction stencil must always include the cell C_i itself. The resulting reconstruction polynomial has k coefficients and is of degree $M = k - 1$. According to the relative position of the stencil elements with respect to the cell C_i for which the reconstruction is undertaken, a stencil is called *centered* (with subscript $(0, e)$), left-sided (with subscript $(-, e)$, the minus sign denoting "left") or right-sided (with subscript $(+, e)$, the plus sign denoting "right"), henceforth. For example, if we take $k = 5$, according to the $WENO_5$ reconstruction procedure for the interface $x_{i+\frac{1}{2}}$, we obtain: The big stencil (refer to Figure (3.1)).

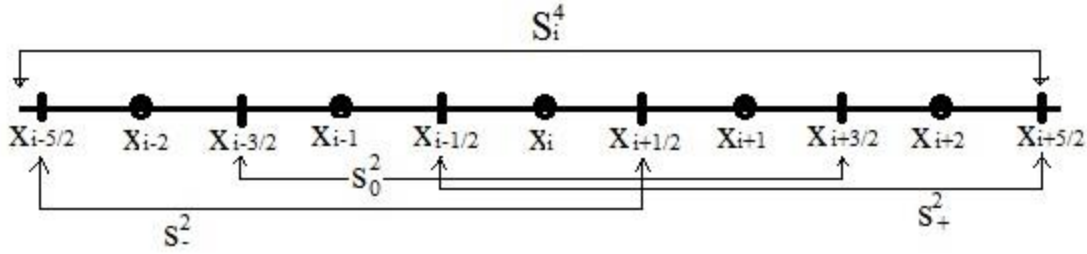


Figure 3.1. $WENO_5$ reconstruction procedure for $x_{i+\frac{1}{2}}$.

The Figure shows the big stencil S_i^4 ,

$$S_i^4 = \{I_{i-2}, I_{i-1}, I_i, I_{i+1}, I_{i+2}\}, \tag{3.5}$$

needed to reconstruct a 4th degree polynomial which is divided into three smaller sub-stencils:

$$\begin{aligned} S^2(-, e) &= \{I_{i-2}, I_{i-1}, I_i\}, \quad S^2(0, e) = \{I_{i-1}, I_i, I_{i+1}\}, \\ S^2(+, e) &= \{I_i, I_{i+1}, I_{i+2}\} \end{aligned} \tag{3.6}$$

where the superscript is the degree of the piece-wise polynomial to be constructed on these sub-stencils. On each sub-stencil a degree 2 polynomial is reconstructed. From now on, we will not explicitly use e in the subscript for ease of notation. It will only be used where necessary. The reconstruction polynomial $P_i^M(x, t^n)$ of degree M is obtained from the known cell averages, W_j^n , by imposing integral conservation i.e., the following must hold:

$$\frac{1}{\Delta x} \int_{C_i} P_i^M(x, t^n) dx = W_j^n, \quad \forall C_i \in S_i^M. \tag{3.7}$$

Therefore, for the WENO method of order k in one space dimension, one needs one big central reconstruction stencil S_i^M of $k = M + 1$ elements and $\frac{M}{2} + 1$ small sub-stencils $S_s^{M/2}, s \in \{0, \pm\}$ composed of $\frac{M}{2} + 1$ elements to reconstruct several lower order polynomials of degree $\frac{M}{2}$.

Here s is the stencil-shift with respect to the central element I_i , denoted by the sign of the shift, $\{0, \pm\}$. The linear WENO reconstruction at the element interface, $x_{i+\frac{1}{2}}$, is then given as a linear combination of the lower order reconstruction polynomials, $P_s^{M/2}(x, t^n)$, obtained from the sub-stencils $S_s^{M/2}$ using the same integral conservation principle, Equation (3.7), above. The linear weights, λ_s are chosen in such a way that the linear combination of the lower order polynomials is identical to the one obtained via the reconstruction polynomial on the big stencil S_i^M . The weights λ_s obviously depend on the position x for which the reconstruction is to be done. For consistency, the sum of the weights must always be equal to unity. Furthermore, the weights λ_s should be positive and must not depend on the solution U_j^n .

Alternatively, for non-smooth solutions, the point value

$$U_{i+\frac{1}{2}}^n = U\left(x_{i+\frac{1}{2}}, t^n\right)$$

is then given by a suitable non-linear combination of the reconstruction polynomials obtained on the sub-stencils. In order to make the WENO scheme non-linear, i.e. data-dependent, the reconstruction at point $x_{i+\frac{1}{2}}$ is obtained by using a nonlinear combination of the lower order reconstruction polynomials of the sub-stencils by substituting the linear weights with nonlinear weights ω_s , which are defined as

$$\omega_s = \frac{\tilde{\omega}}{\sum_s \omega_s}, \quad \tilde{\omega} = \frac{\lambda_s}{(\sigma_s + \epsilon)^r}, \quad s \in \{0, \pm\}, \tag{3.8}$$

where σ_s denotes the so-called smoothness or oscillation indicator, ϵ is a small number to prevent division by zero and r is an exponent for which in Shu and Jiang (1996) $r = 2$ is always chosen. For the smoothness indicator

$$\sigma_s = \sum_{l=1}^{M/2} \int_{x_{i-\frac{1}{2}}}^{x_{i+\frac{1}{2}}} h^{2l-1} \left(\frac{\partial^l}{\partial x^l} P_s^{M/2}\right)^2 dx, \tag{3.9}$$

where $h = \Delta x$ and $P_s^{M/2}(x)$ are polynomials of degree $M/2$ on the sub-stencils, the term h^{2l-1} is used to remove scaling effects from the derivatives as proposed in Shu and Jiang (1996).

For further clarification of the computation of the weights, the following example will be used:

Computing linear weights λ for WENO₃ scheme, performing the reconstruction at point $x_{i+\frac{1}{2}}$, there is one big central stencil with three elements denoted as $S_i^2 = \{I_{i-1}, I_i, I_{i+1}\}$ and two sub-stencils both composed of two elements, denoted as $S_{-1}^1 = \{I_{i-1}, I_i\}$ for the left-side and $S_1^1 = \{I_i, I_{i+1}\}$ for the right-side, respectively. In order to compute the reconstruction polynomial on the big stencil, S_i^2 , we use the integral conservation principle, Equation (3.7), which leads to the second order reconstruction polynomial:

$$P_i^2 = \frac{1}{2}U_{i-1}^n + \frac{5}{6}U_i^n - \frac{1}{6}U_{i+1}^n + (U_i^n - U_{i-1}^n)\xi + \left(\frac{1}{2}U_{i-1}^n - U_i^n + \frac{1}{2}U_{i+1}^n\right)\xi^2, \tag{3.10}$$

where $x = x_{i-1} + \xi\Delta x$. On the two sided sub-stencils, we obtain the following first order polynomials

$$p_{-1}^1(x) = \frac{1}{2}U_i^n + \frac{1}{2}U_{i-1}^n + (U_i^n - U_{i-1}^n)\xi \tag{3.11}$$

and

$$p_1^1(x) = \frac{3}{2}U_i^n - \frac{1}{2}U_{i+1}^n + (U_{i+1}^n - U_i^n)\xi$$

on the left and right side, respectively.

The conditions to obtain the linear weights, λ_{-1} and λ_1 , are then the following system of equations:

$$\begin{cases} \lambda_{-1} + \lambda_1 = 1, \\ p_{-1}^1(x_{i+1/2})\lambda_{-1} + p_1^1(x_{i+1/2})\lambda_1 = P_i^2\left(x_{i+\frac{1}{2}}\right), \end{cases} \quad (3.12)$$

which, after some algebraic manipulations, result in the following linear weights: $\lambda_{-1} = \frac{1}{3}$ and $\lambda_1 = \frac{2}{3}$.

These results are then used to compute the nonlinear weights for each sub-stencil. For instance, to compute the nonlinear weight for the left-sided sub-stencil the procedure should be:

$$\omega_{-1} = \frac{\tilde{\omega}_{-1}}{\sum \omega_s}, \quad \tilde{\omega}_{-1} = \frac{\lambda_{-1}}{(\sigma_{-1} + \epsilon)^r} = \frac{1/3}{(\sigma_{-1} + \epsilon)^r}, \quad (3.13)$$

where $\sum \omega_s$ is the sum of all the nonlinear weights computed for each sub-stencil and

$$\sigma_{-1} = \int_{x_{i-1/2}}^{x_{i+1/2}} h \left(\frac{d(p_{-1}^1(x))}{dx} \right)^2 dx, \quad (3.14)$$

with $h = \Delta x$ and $x = x_{i-1} + \xi \Delta x$.

This original WENO reconstruction of [Shu and Jiang (1996)] for one dimension, described here, is rather difficult to generalize to unstructured triangular and tetrahedral meshes in two and three dimensions because of the need to determine optimal linear weights [Dumbser et al. (2007) and Dumbser and Käser (2007)]. For more details, we refer to [Hu and Shu (1999); Shi and Shu (2002) and Zhang and Shu (2009)]. Therefore, we present, in Section 3.2.2, a different idea that can be more easily extended to unstructured meshes.

3.2.2. Polynomial WENO reconstruction

In this section, we present an alternative reconstruction procedure for the one dimensional case on the basis of a new reconstruction technique, called the arbitrary high order finite volume scheme, proposed by [Dumbser and Käser (2007)], which makes use of techniques developed originally in the discontinuous Galerkin framework. The polynomial WENO reconstruction operator produces entire polynomials, $P_i(x, t^n)$, as the ENO approach proposed by [Harten et al. (1987)].

However, the method is formally written like a WENO scheme given in Liu et al. (1994) and Shu (1997) with a particularly simple choice for the linear weights. The most important difference between this scheme and the classical WENO scheme of [Shu (1997)] is that standard WENO methods reconstruct point values at the Gaussian integration points instead of an entire polynomial valid inside each control volume, $C_i = [x_{i-1/2}, x_{i+1/2}]$. The reconstruction is done

for each element on a reconstruction stencil $S_i^{(s)}$, which is given by the following union of the elements C_i and its neighbors C_j ,

$$S_i^{(s)} = \cup_{j=i+s-e}^{i+s+e} C_j, \tag{3.15}$$

where s is now the stencil shift with respect to the central cell I_i and e is the spatial extension of the stencil to the left and the right. A central reconstruction stencil ($s = 0$), an entirely left-sided stencil ($s = -e$) and an entirely right-sided stencil ($s = e$) are given, respectively, by

$$S_i^{(0)} = \cup_{j=i-e}^{i+e} C_j, \quad S_i^{(-e)} = \cup_{j=i-2e}^i C_j \tag{3.16}$$

and

$$S_i^{(+e)} = \cup_{j=i}^{i+2e} C_j,$$

which are the three fixed reconstruction stencils which we adopt. As usual for finite volume schemes, data are represented by the cell averages of a conserved quantity, U , inside cell C_i . Now that the stencils have been established, the use of e will be dropped for ease of notation. In order to achieve high order accuracy for the spatial discretization, one looks for a spatial reconstruction polynomial P obtained from $S_i^{(s)}$ at time t^n . The reconstruction polynomial for element I_i is written as

$$P_i^{(s)}(\xi, t^n) = \sum_{l=0}^M \phi_l(\xi) \hat{w}_l^{(s)}(t^n), \tag{3.17}$$

where ξ is the coordinate in a reference coordinate system. On the right hand side of Equation (3.17) the standard tensor index notation is used. For each element I_i , a reference coordinate $\xi \in [0,1]$ is used. The transformation from the physical coordinate system into the reference coordinate system ξ is defined by

$$x = x_{i-\frac{1}{2}} + \xi \Delta x. \tag{3.18}$$

The reconstruction basis, $\phi_l(\xi)$, is composed of polynomials of degree M and depends on space. As basis functions, the Legendre polynomials,

$$\phi_l(\xi) = (l!)^{-1} \frac{d^l}{d\xi^l} [(\xi^2 - \xi)^l] \tag{3.19}$$

are used on the unit interval, which form an orthogonal basis with respect to the inner product:

$$\langle \phi_i(\xi), \phi_k(\xi) \rangle = \int_0^1 \phi_i(\xi) \phi_k(\xi) d\xi . \tag{3.20}$$

In what follows, standard tensor index notation is used, implying summation over indices appearing twice. The number of polynomial coefficients (degrees of freedom) is $k = M + 1$, where M is the degree of the reconstruction polynomial and k is the spatial order of accuracy of

the scheme in space. To compute the reconstruction polynomial, $P_i(\xi, t^n)$, valid for element I_i , one requires the integral conservation for all elements I_j inside the stencil $S_i^{(s)}$, i.e.,

$$\int_{I_j} P_i^{(s)}(\xi, t^n) d\xi = \int_{I_j} \phi_l(\xi) d\xi \cdot \widehat{\omega}_l^{(s)}(t^n) = U_j^n, \quad \forall I_j \in S_i^{(s)}. \quad (3.21)$$

Equation (3.21) yields a system of linear equations for the unknown coefficients $\widehat{\omega}_l^{(s)}$ of the reconstruction polynomial on stencil $S_i^{(s)}$ that can be easily solved.

To obtain the final non-oscillatory reconstruction polynomials for each element I_i at the time t^n , a data-dependent nonlinear combination of the polynomials $P_i^{(-)}(\xi, t^n)$, $P_i^{(0)}(\xi, t^n)$ and $P_i^{(+)}(\xi, t^n)$ obtained from the central, left-sided and right-sided stencils is constructed as follows:

$$P_i(\xi, t^n) = \widehat{\omega}_l(t^n) \phi_l(\xi), \quad (3.22)$$

where

$$\widehat{\omega}_l(t^n) = \omega_0 \widehat{\omega}_l^{(0)}(t^n) + \omega_- \widehat{\omega}_l^{(-)}(t^n) + \omega_+ \widehat{\omega}_l^{(+)}(t^n).$$

Hence,

$$P_i(\xi, t^n) = \omega_- P_i^{(-)}(\xi, t^n) + \omega_0 P_i^{(0)}(\xi, t^n) + \omega_+ P_i^{(+)}(\xi, t^n). \quad (3.23)$$

The nonlinear weights $\omega_{(s)}$, $s \in \{0, \pm\}$ are given by the relations

$$\omega_s = \frac{\widetilde{\omega}}{\sum_s \omega_s}, \quad \widetilde{\omega} = \frac{\lambda_s}{(\sigma_s + \epsilon)^r}; \quad s \in \{0, \pm\}. \quad (3.24)$$

The oscillation indicators σ_s are computed as for point-wise WENO reconstructions:

$$\sigma_s = \sum_{l=1}^M \int_0^1 \left(\frac{\partial^l}{\partial \xi^l} P_i^{(s)}(\xi, t^n) \right)^2 d\xi. \quad (3.25)$$

The parameters ϵ and r are constants for which one typically chooses $\epsilon = 10^{-14}$ and $r = 8$. Unlike the nonlinear weights used in the usual point-wise WENO reconstruction, the linear weights λ_s are simply defined by $\lambda_- = \lambda_+ = 1$ and a very large linear weight λ_0 on the central stencil, typically $\lambda_0 = 10^5$ as presented in [Shu and Jiang (1996)], show that the numerical solutions are quite insensitive to the WENO parameters ϵ and r . In Dumbser et al. (2007) it is shown that the numerical results are also insensitive to the linear weights on the central stencil λ_0 . Typically, in order to avoid spurious oscillations that may appear when applying ENO or WENO reconstruction operators component-wise to non-linear hyperbolic conservation systems, the reconstruction needs to be done on characteristic variables [Harten et al. (1987)]. The result of reconstruction is a non-oscillatory spatial polynomial $P_i(\xi, t^n)$ defined at t^n inside each spatial element I_i . The advantage of the polynomial WENO reconstruction is its straightforward extension to general unstructured meshes. The inconvenience is that at a given order of accuracy k the total stencil needed for the reconstruction is wider than the one of the classical point-wise

WENO. In the following section, the alternative polynomial WENO reconstruction to the one described in this section is applied. Specifically, the third order polynomial WENO reconstruction is employed, the rescaled Legendre polynomials up to degree two are used as reconstruction basis functions, which according to Equation (3.19) are

$$\phi_0(\xi) = 1, \quad \phi_1(\xi) = 2\xi - 1 \quad \text{and} \quad \phi_2(\xi) = 1 - 6\xi + 6\xi^2. \quad (3.26)$$

It can be easily checked that the set of non-zero functions $\{\phi_l(\xi): l = 0, 1, 2\}$, given above, is mutually orthogonal on the unit interval $[0, 1]$. Following Equations (3.22)-(3.25), we obtain the following expansion coefficients (note that $e = 1$):

- for the left-sided stencil

$$\begin{aligned} \hat{\omega}_0^{(-1)} &= U_i^n, \quad \hat{\omega}_1^{(-1)} = \frac{1}{4}U_{i-2}^n - U_{i-1}^n + \frac{3}{4}U_i^n, \\ \hat{\omega}_2^{(-1)} &= \frac{1}{12}U_{i-2}^n - \frac{1}{6}U_{i-1}^n + \frac{1}{12}U_i^n, \end{aligned} \quad (3.27)$$

- for the central stencil

$$\begin{aligned} \hat{\omega}_0^{(0)} &= U_i^n, \quad \hat{\omega}_1^{(0)} = -\frac{1}{4}U_{i-1}^n + \frac{1}{4}U_{i+1}^n, \\ \hat{\omega}_2^{(0)} &= \frac{1}{12}U_{i-1}^n - \frac{1}{6}U_i^n + \frac{1}{12}U_{i+1}^n, \end{aligned} \quad (3.28)$$

- and for the right-sided stencil

$$\begin{aligned} \hat{\omega}_0^{(1)} &= U_i^n, \quad \hat{\omega}_1^{(1)} = -\frac{3}{4}U_i^n + U_{i+1}^n - \frac{1}{4}U_{i+2}^n, \\ \hat{\omega}_2^{(1)} &= \frac{1}{12}U_i^n - \frac{1}{6}U_{i+1}^n + \frac{1}{12}U_{i+2}^n. \end{aligned} \quad (3.29)$$

The oscillation indicator is given by

$$\sigma_{(s)} = 156\left(\hat{\omega}_2^{(s)}\right)^2 + 4\left(\hat{\omega}_1^{(s)}\right)^2, \quad s \in \{-1, 0, 1\}. \quad (3.30)$$

3.2.3. The ADER-Finite Volume One step Scheme

For time integration, it is important to take into account the efficiency and accuracy of time integration schemes. Several studies focus on the efficiency of Runge-Kutta (RK) time discretization schemes, Bijl et al. (2001). However it is found that the efficiency of these schemes decreases substantially if, due to the so-called Butcher barriers [Butcher (2005)], the order of accuracy becomes greater than four, which makes the number of intermediate RK stages larger than the formal order of accuracy.

In order to achieve an arbitrarily accurate time discretization, we apply the arbitrary high order derivation (ADER) approach, developed originally and introduced in Toro et al. (2001), to the

semi-discrete form of the system resulting from the integration in the reference system. The ADER approach consists of a Taylor expansion in time, the solution of generalized Riemann problems (GRP) to approximate the space derivatives at the interface and the Cauchy-Kovalewski procedure for replacing the time derivatives in the Taylor series by space derivatives. Throughout our work, the approach in Dumbser et al. (2007) with regard to the ADER for high order time integration of the finite volume method on unstructured grids, called ADER-FV scheme, is followed. The difference is that in Dumbser et al. (2007) the ADER is simplified for general linear hyperbolic systems, while in our work the original approach for the general nonlinear hyperbolic systems is applied [Pedro et al. (2014)].

Considering a general nonlinear system of conservation laws where U is a vector of conserved variables and $F(U)$ is a vector of nonlinear fluxes, once all basis functions are given in the reference coordinate, we apply the Cauchy-Kovalewski procedure in the reference element, rewriting the generic nonlinear hyperbolic system of conservation laws directly as

$$\frac{\partial U}{\partial t} + \Delta t \frac{\partial}{\partial \xi} F^*(U) = 0 \quad (3.31)$$

with

$$F^* = F \xi_x. \quad (3.32)$$

The iterative steps can be summarized as follows:

1. Compute $F(q)$,
2. Compute the flux F^* in the reference space,
3. Perform the local space-time discontinuous Galerkin interaction.

Further details of the approach can be found in Titarev and Toro (2002); Titarev and Toro (2005), and references contained therein.

3.3. Staggered approach

The staggered approach with a structure predictor is considered here, [Blom (1998); Lefrançois and Boufflet (2010)]. The algorithm is such that at time t^n the state of both the fluid and the structure, and also the state of the mesh are known. Therefore, the next steps are concerned to integrate the fluid-structure system from the current time t^n to t^{n+1} :

1. At t^{n+1} the state of the structure is predicted,
2. By using the predicted state of the structure the fluid is integrated at t^{n+1} ,
3. By using the fluid pressure on the boundary the structure is update at t^{n+1} .

3.3.1. Artificial added mass instabilities

Staggered schemes present an inherent instability when applied to couple structure and incompressible fluid [Conca et al. (1997) and Förster et al. (2007)]. In this paper a compressible fluid is considered, therefore the added mass effect is not considered. However two different structure predictors of different order of accuracy are considered, taking into account that the

structure predictor is one of the important features which influences the instabilities in sequential staggered schemes [Förster et al. (2007)].

3.3.2. Structure Predictors

The fluid is modeled by the Euler Equations (2.3) and integrated by the schemes presented in Section 3.2 and the structure governed by the mass-spring system, Equation (4.2), is integrated by the schemes presented in Section 3.1. To predict the structure we use the first order predictor [Blom (1998)]:

$$\dot{q}^{n+1} = \dot{q}^n + \Delta t \ddot{q}^n, \quad (3.33)$$

which will be denoted by *Predictor B*. We test also one of the predictors used in a FSI problem applied to the oscillating aerofoil in inviscid flow, [Piperno (1997)], namely the linear structure predictor

$$q^{n+1} = q^n + \Delta t \dot{q}^n + \frac{1}{2} \Delta t^2 \ddot{q}^n, \quad (3.34)$$

which will be denoted by *Predictor P*.

In the next section a discussion of the results of applying the approaches recommended in this section will be presented.

4. Numerical tests and results

The case study presented in Section 2 will be considered as a test example. Numerical aspects will be tested. Specifically the performance of the time integration schemes on structural dynamics will be tested first. Different strengths of these approaches will be summarized. Thereafter a discussion of the coupling procedures will be presented. Two predictors as presented in Section 3 are tested and discussed. Finally the complete coupled system is discussed. The good performance of the high-order schemes is clearly evident.

4.1. Structural Dynamics Simulations

We test the performance of the ESDIRK, for the structure dynamics simulations, compared with the second order Newmark $\left(\beta = \frac{1}{4}, \gamma = \frac{1}{2}\right)$. As discussed in Section 1, the Newmark $\left(\beta = \frac{1}{4}, \gamma = \frac{1}{2}\right)$ is the most used to integrate structure when it comes to applying a staggered approach for fluid-structure interaction problems. This scheme is the optimal version of the Newmark methods with no numerical damping and unconditionally stable [Bathe (1976)]. However, in Bardella et al. (2003) it was found that this scheme is affected by a significant drift error measured by

$$d_2 = \frac{\omega^2 \Delta t}{A} \lim_{T \rightarrow \infty} \left[\frac{1}{T} \left(q^{exact}(T) - q^{alg}(T) \right) \right], \quad (4.1)$$

where ω is the undamped angular frequency, A is the amplitude of the system and T is the total time integration. In Zuijlen and Bijl (2005), it was found that this drift reduces for ESDIRK schemes.

In this section, we integrate directly the harmonic oscillator

$$m\ddot{q} + kq = f_{ext}(t), \quad (4.2)$$

where m is the mass, k is the spring stiffness and $f_{ext}(t)$ is the external force, which can be either zero or a periodic forcing term. As test examples, we consider examples presented in Zuijlen and Bijl (2005) and in Bardella et al. (2003).

1. The first test example is a free mass with periodic forcing $m\ddot{q} + kq = f_{ext}(t)$, with $m = 1$, $k = 0$ and under a periodic loading $f_{ext}(t) = A\sin(\omega t)$. This example was tested in Bardella et al. (2003) and in Zuijlen and Bijl (2005). Therefore, as in those two papers we also use $A = 100$ and $\omega = 1$. The initial conditions are given by $q(0) = -A$ and $\dot{q}(0) = -A$, where A is the amplitude of the vibrations.
2. The second test example is an unforced mass-spring system $m\ddot{q} + kq = 0$, with $m = 1$, under the initial condition $q(0) = 1$ and $\dot{q}(0) = 0$. This example served as test in Zuijlen and Bijl (2005).

Figures 4.1-4.2 show the results for the displacement in time by Newmark $_{\beta}$ scheme and by ESDIRK schemes from third to fifth order. It is possible to see that the drift error is more distinctive for the Newmark $_{\beta}$ scheme, which is exactly the same as the cases reported in Zuijlen and Bijl (2005) and [Bardella et al. (2003)].

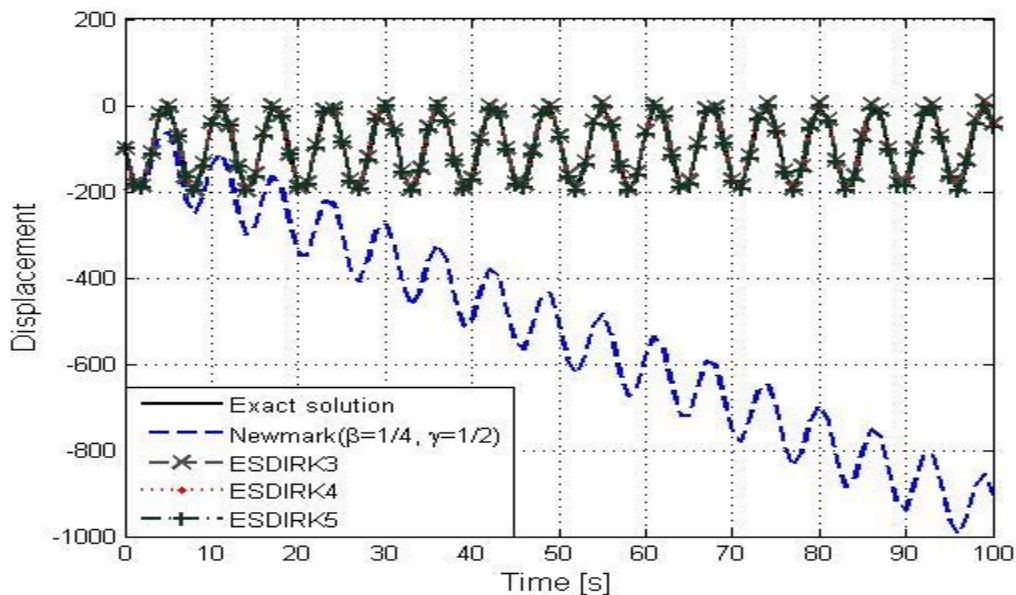


Figure 4.1. Integration of the free mass equation for sinusoidal acceleration $\ddot{q} = 100\sin(t)$, $\Delta t = 1$, subject to $q_0 = -100$ and $\dot{q}(0) = -100$

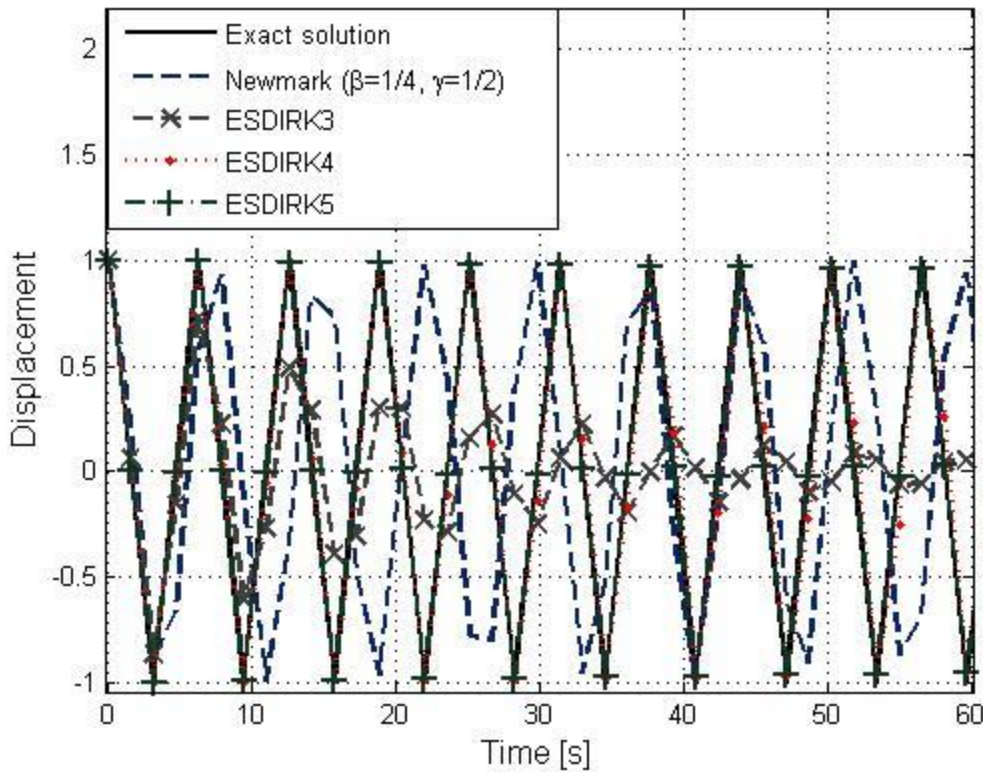


Figure 4.2. Integration of the harmonic oscillator $\ddot{q} + \omega^2 q = 0$ $\Delta t = 1$, subject to $q_0 = 0$ and $\dot{q}(0) = 1$

Table 4.1 shows the drift error that affects the Newmark $_{\beta}$ scheme and the ESDIRK schemes, for the data $A = 100$, $\omega = 1$, $\Delta t = 1$ and $\Delta t = 0.1$ by setting $T = 100$. The parameter p , which denotes the observed order of accuracy, is computed by

$$p = \ln \frac{(\|d_{4\tau} - d_{2\tau}\|_2)}{(\|d_{2\tau} - d_{1\tau}\|_2)}, \tag{4.3}$$

where d is the computed structural displacement on meshes of different time-step sizes, denoted by τ , 2τ and 4τ , and the L_2 norm is used to measure the differences. In the last column is given CPU time needed by our code, in MATLAB 7.0, on a Intel(R) Core(TM)2 Duo CPU T6570 at 2.10GH $_z$ with 3.00 GB of RAM, and 32 bit operating system.

Table 4.1. Drift error affecting various integration schemes for the data of Figure 4.1

Scheme	$ d_2 , \Delta t = 1$	$ d_2 , \Delta t = 0.1$	Order of temporal accuracy p	Time-CPU(sec.)
Newmark $_{\beta}$	8.56×10^{-2}	842×10^{-4}	3.00	88.327
ESDIRK3	6.88×10^{-4}	1.0×10^{-7}	4.5	285.417
ESDIRK4	3.92×10^{-4}	3.0×10^{-10}	5.0	285.496
ESDIRK5	1.4×10^{-7}	0.00	6.005	286.509

4.2. Numerical Results for FSI

The parameters for the piston problem are given in Table 4.2, and they are taken in a similar way as in Lefrançois and Boufflect (2010). The characteristic time-scales for fluid, structure and fluid structure interaction system are denoted by

$$T_f = \frac{L_0}{c}, T_s = 2\pi \sqrt{\frac{m}{k}}, \quad T_{fs} = \frac{2\pi}{\omega_{fs}}, \quad (4.4)$$

respectively. The relation $\frac{T_s}{T_f}$ determines the importance of the transient effects on the fluid behaviour, [Lefrançois and Boufflect (2010)],

- If $T_s \approx T_f$ the coupling can be considered as strong.
- If $T_s \gg T_f$ the fluid can be considered as stead.

Table 4.2. Parameters for the piston problem

L_0	1 m
q^0	0.2 m
L_{s0}	1.2 m
m	10 Kg
k	1×10^7 N/m
p_0	1×10^5 Pa
γ	1.4
c_0	334 m/s

Therefore, taking into account the parameters in Table 4.2, $T_s \approx T_f$, so the coupling is considered *strong*, [Garelli (2011)]. Figure 4.3 shows the displacement and the total energy computed with a staggered approach where the Newmark $_{\beta}$ scheme and the ESDIRK schemes are used as structure solvers. The results show that the amplitude of the oscillations reduce in time for ESDIRK because of the decreasing of the energy in time. The curves become more damped as CFL number increases, as it is shown in Figure 4.4. An alternative to decrease the additional fictitious energy consists in introducing more accurate structural predictors. Figure 4.5 shows the structural displacement and the structural total energy computed using ESDIRK5 as structural solver, where the coupled algorithm is applied to the structural predictor given by Equation (3.34). We can see that the results improved significantly, showing the better performance of predictor Equation (3.34) compared with the predictor Equation (3.33).

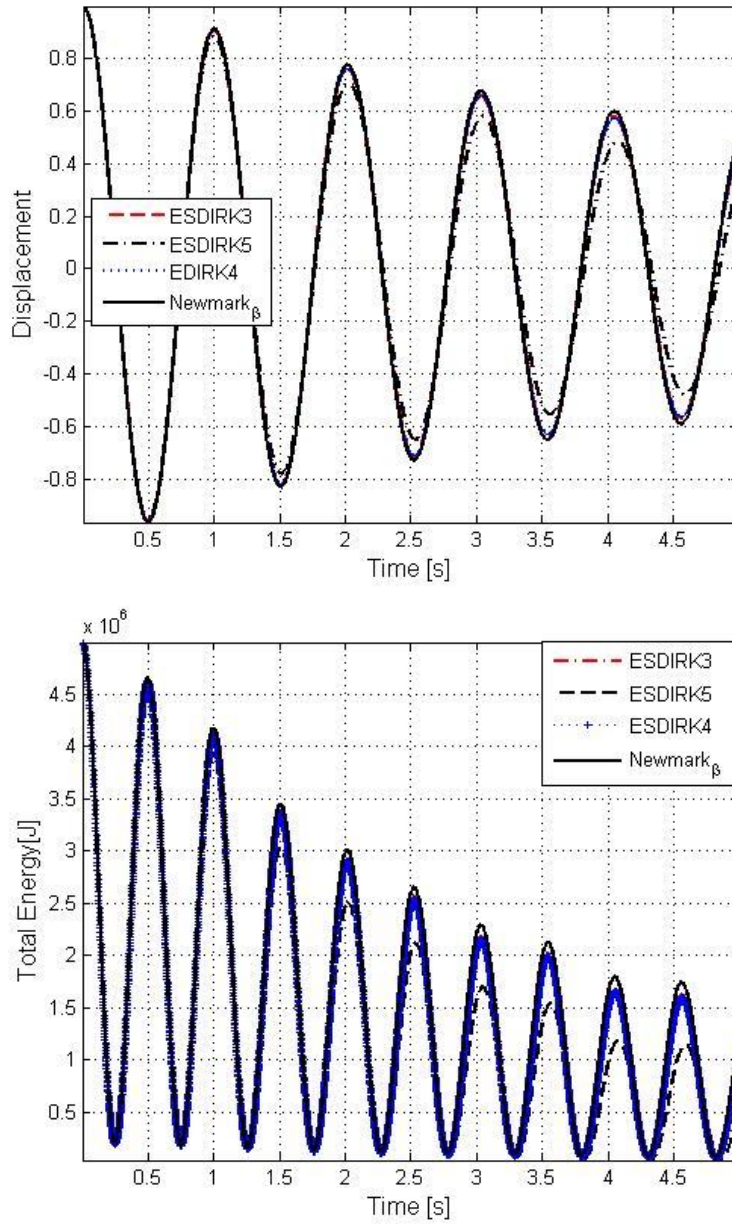


Figure 4.3. Piston displacement (top) and structure total energy (bottom) computed by a staggered approach. Newmark $_{\beta}$ and ESDIRK schemes are used to integrate the structure

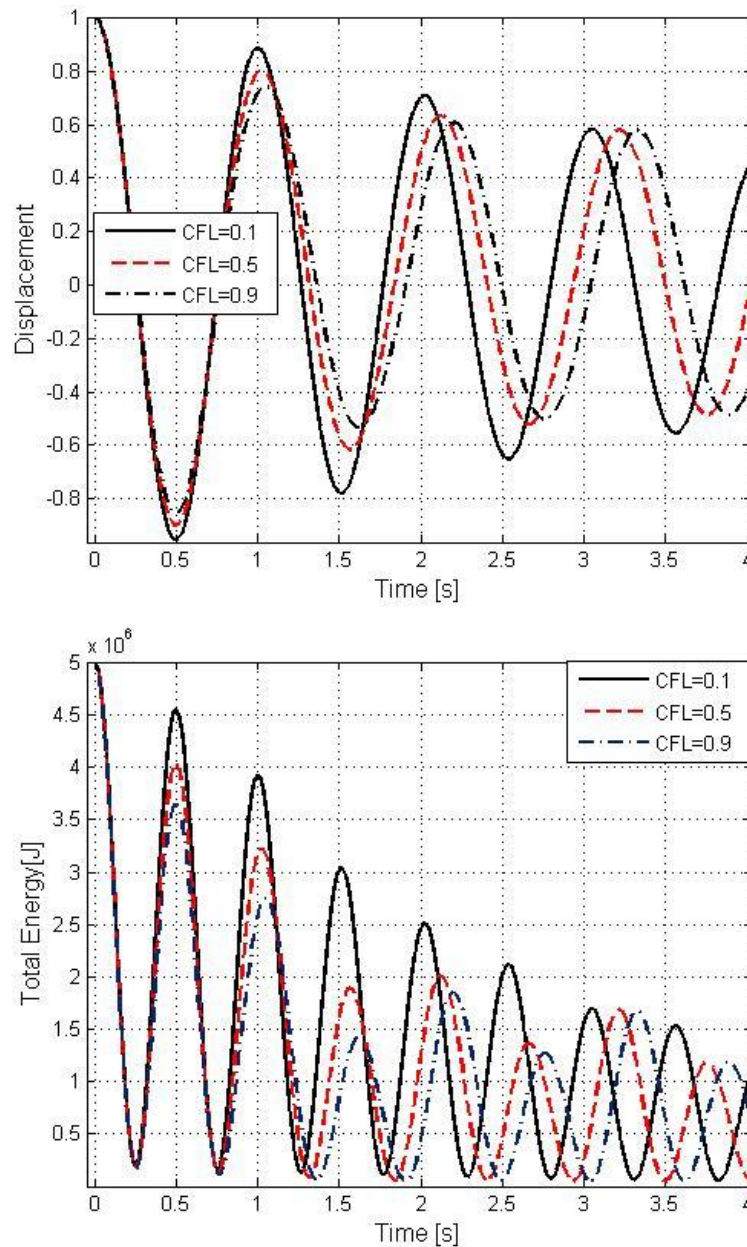


Figure 4.4. Displacement of the structure (top) and the structure total energy (bottom) computed using ESDIRK with predictor Equation (3.33) for different CFL numbers

4.3. Energy Conservation

We have computed the structural energy in Section 4.2; however the concern in identifying and applying adequate structure predictors is to reduce considerably the energy conservation errors, [Piperno (1997)]. In this section we discuss the efficiency of the staggered scheme used with a structural predictor. This quality indicator for the efficiency of the scheme can be derived through the integration, on the domain $[0, L(t)]$, the third conservation law from Equation (2.5), such that

$$\frac{\partial}{\partial t} \int_0^{L(t)} \rho E A dx + A[u(\rho E + p) - \rho E \omega_x]_0^{L(t)} = 0. \quad (4.5)$$

Taking into account the boundary conditions

$$u(L(t), t) = \omega_x(L(t), t) = \dot{q}(t) \text{ and } u(0, t) = \omega_x(0, t) = 0 \quad (4.6)$$

and integrating Equation (4.5) in time between the initial condition and the current time t yields

$$\int_0^{L(t)} \rho A E dx - \int_0^{L(0)} \rho A E dx = - \int_0^t A p(L, t) u(L, t) dt. \quad (4.7)$$

Equation (4.5) is called impulsion [Lefrançois and Bufflect (2010)], and is usually denoted by $I(t)$. It corresponds to the total energy variation (on left-hand term) or the fluid energy required for the motion of the piston [Lefrançois and Bufflect (2010)]. On the other hand, integrating in time the mass-spring system Equation (4.2), we can define the piston mechanical energy variation,

$$E(t) - E(0), \text{ where } E(t) = \frac{1}{2} m \dot{q}^2 + \frac{k}{2} (L_{se} - q(t) + L_{s0})^2. \quad (4.8)$$

There are two components for the mechanical energy: the kinetic component, denoted here by $E(t)_c$, and the potential component, denoted by $E(t)_p$.

The energy conservation is satisfied if

$$I(t) = E(t) - E(0) \text{ for } t \geq 0, \quad (4.9)$$

where from the initial conditions $q(x, 0) = q^0$ and $\dot{q}(x, 0) = 0$,

$$E_0 = \frac{1}{2} k (L_{se} - q(x, 0) + L_{s0})^2. \quad (4.10)$$

Equation (4.7) is computed using the fluid solver and Equation (4.8) is computed using the structure solver.

Figures (4.7), shows energy conservation, by using *Predictor* (top) and by using *Predictor P* (bottom), respectively, in both cases taking $m = 100$. As shown the mechanical energy (denoted by E/E_0), and the impulsion (denoted by I/E_0), move in opposite directions which is a reflection of what is expected in such a physical setting. Therefore, the energy is conserved. The variation of the mechanical energy indicates the transfer of the energy from the structure to the fluid. This behavior can also be seen when $m = 10 \text{ Kg}$, as shown by Figure 4.6 at the bottom we can do the same analysis on the left-hand side for *Predictor B* and on the right-hand side for *Predictor P*.

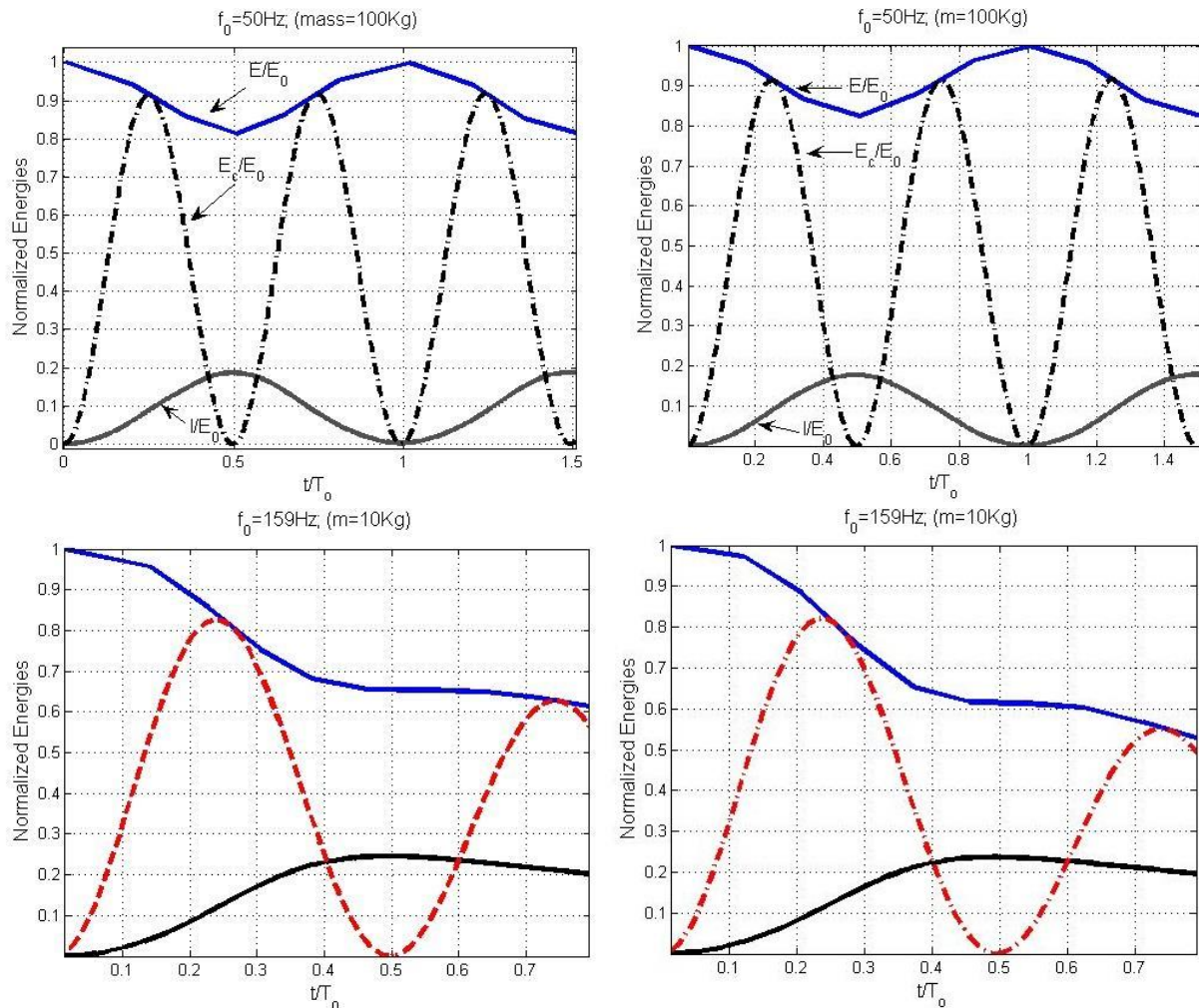


Figure 4.6. Energy conservation: The results are computed by using ESDIRK3 as structural solver and structural predictors: *Predictor B* (left hand side) and *Predictor P* (right-hand side). Here $m = 100$, on top and $m = 10$ on bottom

5. Concluding Remarks

A staggered approach with structure predictor was considered to solve an FSI problem in which the piston problem was considered as a case study. The fluid was modeled by the nonlinear Euler equations written in moving mesh coordinates by the arbitrary Lagrangian Euler (ALE) formulation and the structure by the mass-spring system. The fluid domain was discretized by the arbitrary high order finite volume schemes. The structure was integrated by the Newmark $_{\beta}$ and ESDIRK3-5 schemes and two structure predictors were applied. ESDIRK schemes showed superior results with both predictors. From the results obtained it is believed that ESDIRK can be used as structure solver for FSI problems in place of the usual Newmark $_{\beta}$ method. The higher computational time consuming of ESDIRK schemes is compensated by their higher order of accuracy.

Acknowledgements

This work is based on the research supported in part by the National Research Foundation of South Africa UID: 85566.

JC Pedro would like to acknowledge funding from Angolan Department of Science and Technology.

REFERENCES

- Bardella, L., Carini, A. and Genna, F. (2003). Time integration errors and some new functionals for the dynamics of a free mass, *Comp. Struct.*, Vol. 81, pp. 2361–2372
- Bathe, K. J. and Wilson, E. L. (1976). Numerical Methods in Finite Element Analysis, Prentice-Hall, Englewood Cliffs, NJ.
- Bijl, H., Carpenter, M. H. and Vatsa, V. N. Time integration Schemes for Unsteady Navier Stokes Equations, *15th Computational Fluid Dynamics Conference, AIAA*, pp.2001–2612.
- Blom, F. J. (1998). A monolithical fluid-structure interaction algorithm applied to the piston problem, *Computer methods in applied mechanics and engineering*, Vol. 167, pp. 369–391.
- Butcher, J. C. (2005). The numerical analysis of ordinary differential equations: Runge-Kutta and General Linear Methods, *Computers & Structures*, Vol. 83, pp. 93–105.
- Conca, C., Osses, A. and Planchard, J. (1997). Added Mass and Damping in Fluid-Structure Interaction, *Computer Methods in Applied Mechanics and Engineering*, Vol. 146, pp. 387–405.
- Donea, J., Giuliani, S. and Halleux, J. P. (1982). An arbitrary Lagrangian Eulerian finite element method for transient dynamic fluid-structure interactions, *Comp. Methods Appl. Mech. Engrg.*, Vol. 33, pp. 689–723.
- Dumber, M., äser, M, Titarev, V. and Toro, E. F. (2007). Quadrature-free non-oscillatory finite volume schemes on unstructured meshes for nonlinear hyperbolic systems, *Journal of Computational Physics*, Vol. 226, pp. 204–243.
- Dumbser, M. and Käser, M. (2007). Arbitrary high order non-oscillatory finite volume schemes on unstructured meshes for linear hyperbolic systems, *Journal of Computational Physics*, Vol. 221, pp .693–723.
- Farhat, C. and Lesoinne, M. (2000). Two efficient staggered algorithms for the serial and parallel solution of three-dimensional nonlinear transient aeroelastic problems, *Computer methods in applied mechanics and engineering*, Vol. 182, pp. 499–515.
- Farhat, C., Geuzaine, P., and Grandmont, C. (2001). The Discrete Geometric Conservation Law and the Nonlinear Stability of ALE Schemes for the Solution of Flow Problems on Moving Grids, *Journal of Computational Physics*, Vol. 174, pp. 669-694.
- Förster, C., Wall, W. A. and Ramm, E. (2007). The Artificial Added Mass Effect in Sequential Staggered Fluid-Structure Interaction Algorithms, *Computer Methods in Applied Mechanics and Engineering*, Vol. 196, pp. 1278–1293.
- Garelli, L. (2011). Fluid Structure Interaction using Arbitrary Lagrangian Eulerian Formulation, Tesis de Doctorado, Facultad de Ingeniería y Ciencias Hídricas, Universidad Nacional del Litoral, Argentina.

- Harten, A., Engquist, B., Osher, S. and Chakravarthy, S. (1987). Uniformly high order essentially non-oscillatory schemes, III, *Journal of Computational Physics*, Vol. 71, pp. 231–303.
- Hu, C. and Shu, C. W. (1999). Weighted essentially non-oscillatory schemes on triangular meshes, *Journal of Computational Physics*, Vol. 150, pp. 97–127.
- Kennedy, C. A. and Carpenter, M. H. (1987). Additive Runge-Kutta schemes for convection diffusion-reaction equations, Wiley-Interscience, New York, NY, USA. 17
- Lefrançois, E. and Boufflet, J. P. (2010). An introduction to Fluid-Structure Interaction: Application to the Piston Problem, *SIAM REVIEW*, Vol. 52, pp. 747–767.
- Liu, D., Osher, S. and Chan, T. (1994). Weighted essentially non-oscillatory schemes, *Journal of Computational Physics*, Vol. 115, pp. 200–212.
- Michler, C., Hulshoff, S. J., van Brummelen, and de Borst, R. (2004). A monolithic approach to fluid-structure interaction, *Computers & fluids*, Vol. 33, pp. 839–848.
- Michler, C., van Brummelen, Hulshoff, S. J. and de Borst, R. (2003). The relevance of conservation for stability and accuracy of numerical methods for fluid-structure interaction, *Computer methods in applied mechanics and engineering*, Vol. 192, pp. 4195–4215.
- Mouro, J. (1996). Interactions fluid structure en grands déplacements, résolution numérique et application aux composants hydrauliques automobiles, Ph. D. Thesis, Ecole Polytechnique, France.
- Park, K. C., Felipa, C. A. and DeRuntz, J. A. (1977). Stabilization of staggered solution procedures for fluid-structure interaction analysis, *Comput. Methods Fluid-Structure Interaction Problems*, AMD.
- Pedro, J. C. and Sibanda, P. (2012). An algorithm for the Strong-Coupling of the Fluid-Structure Interaction Using a Staggered Approach, *International Scholarly Research Network. ISRN Applied Mathematics*, Article ID 391974, 14 pages, doi:10.5402/2012/391974.
- Pedro, J. C., Banda, M.K. and Sibanda, P. (2014). On one-dimensional arbitrary high-order WENO schemes for systems of hyperbolic conservation laws, *Comp. and App. Math.*, vol. 33, pp. 363–384.
- Piperno, S. (1997). Explicit/Implicit Fluid/Structural Staggered Procedures with a Structural Predictor and Fluid Subcycling for 2D Inviscid Aeroelastic Simulations, *International Journal for Numerical Methods in Fluids*, Vol. 25, pp. 1207–1226.
- Piperno, S., Farhat, C. and Larrouturou, B. (1995). Partitioned procedures for the transient solution of coupled aeroelastic problems. Part I: Model problem, theory and two-dimensional application, *Computers methods in applied mechanics and engineering*, Vol. 124, pp. 79–112.
- Prananta, B. B. and Houjet, M. H. L. (1996). Aeroelastic simulation with advanced CFD methods in 2D and 3D transonic flow, Proc. Unsteady Aerodynamics Conference Royal Aeronautical Society, London.
- Shi, J., Hu, C. and Shu, C. W. (2002). A technique of treating negative weights in WENO schemes, *Journal of Computational Physics*, Vol. 175, pp. 108–127.
- Shu, C. W. (1997). Essentially Non-Oscillatory and Weighted Essentially Non-Oscillatory Scheme for Hyperbolic Conservation Laws, NASA/CR-97-206253 ICASE Report N. 97–65.
- Shu, C. W. and Jiang, G. S. (1996). Efficient implementation of Weighted ENO Schemes, *Journal of Computational Physics*, Vol. 126, pp. 202–228.
- Souli, M., Ouahsine, A. and Lewin, L. (2000). ALE formulation for fluid-structure interaction, *Computer methods in applied mechanics and engineering*, Vol. 190, pp. 659–675.

- Titarev, V. A. and Toro, E. F. (2002). Solution of the generalized Riemann Problem for advection-reaction equations, *Proceedings of Royal Society of London*, pp. 271–281.
- Titarev, V. A. and Toro, E. F. (2005). ADER schemes for scalar hyperbolic conservation laws with source terms in three space dimensions, *Journal of Computational Physics*, Vol.202, pp. 196–215.
- Titarev, V. A. and Toro, E. F. (2005). ADER schemes for three-dimensional nonlinear hyperbolic systems, *Journal of Computational Physics*, Vol. 204, pp. 715–736.
- Toro, E. F. , Millington, R. C. and Nejad, L. A. M. (2001). Towards very high order Godunov schemes, E. F. Toro (Ed.), *Godunov Methods, Theory and Applications*, Kluwer/Plenum Academic Publishers, pp. 905–938.
- Zhang, Y. T. and Shu, C. W. (2009). Third order WENO schemes on three dimensional tetrahedral meshes, *Communications in Computational Physics*, Vol. 5, pp. 836–848.
- Zuijlen, A. v. and Bijl, H. (2005). Implicit and explicit higher order time integration schemes for structural dynamics and fluid-structure interaction computations, *Computers & Structures*, Vol. 83, pp. 93–105.